ELSEVIER

Materials Science and Engineering A353 (2003) 133–139

MATERIALS SCIENCE & ENGINEERING A

www.elsevier.com/locate/msea

Precipitation in neutron-irradiated Fe–Cu and Fe–Cu–Mn model alloys: a comparison of APT and SANS data

M.K. Miller [a,*], B.D. Wirth [b], G.R. Odette [c]

[a] *Microscopy, Microanalysis and Microstructure Group, Metals and Ceramics Division, Oak Ridge National Laboratory, P.O. Box 2008, Oak Ridge, TN 37831-6136, USA*

[b] *Lawrence Livermore National Laboratory, P.O. Box 808, L-353, Livermore, CA 94551, USA*

[c] *Department of Mechanical and Environmental Engineering, University of California-Santa Barbara, Santa Barbara, CA 93106, USA*

Abstract

The size, number density and compositions of ultrafine copper–manganese precipitates that form in Fe–0.80at.% Cu and Fe–0.78at.% Cu–1.05at.% Mn model alloys that were neutron irradiated to a fluence of $\sim 1 \times 10^{23}$ nm^{-2} ($E > 1$ MeV) at 288 °C have been estimated by atom probe tomography and small-angle neutron scattering (SANS) experiments. The number density of precipitates was approximately an order of magnitude higher in the Fe–Cu–Mn alloy than in the Fe–Cu alloy. A direct comparison of the microstructural parameters estimated by each technique revealed good agreement between the radii of gyration and the number densities. However, the copper content in precipitates inferred from SANS was significantly higher than estimated from the atom probe results.

Keywords: Atom probe; Small-angle neutron scattering; Microstructural characterization; Neutron irradiation; Precipitation

PACS numbers: 61.82.Bg; 61.12.Ex

1. Introduction

Atom probe field ion microscopy/atom probe tomography (APFIM/APT) [1] and small-angle neutron scattering (SANS) [2] have had important roles in the microstructural characterization of neutron-irradiated reactor pressure vessel steels and related model alloys. Although APT and SANS techniques are based on different principles of operation, several common microstructural parameters may be estimated. The important common parameters include the size of precipitates, as estimated in terms of the radius of gyration and the related Guinier radius, their number densities and compositions. These techniques have provided indispensable data on some of the causes of the embrittlement that occur in these materials. APT and SANS have clearly revealed that nanometer-scale copper–manganese–nickel precipitates are formed in pressure vessel steels and model alloys during neutron irradiation and these precipitates are also enriched in silicon, phosphorus and possibly vacancies [3–5]. The precise nature of these nanometer precipitates is influenced by the composition of the steel, the thermal heat treatments prior to irradiation and the neutron irradiation conditions.

In this study, the effect of manganese additions on the size, composition and number density of copper-enriched precipitates has been investigated in model alloys with a combination of APT and SANS. These independent estimates on the identical materials should also enable some of the assumptions that are used in the interpretation of the data to be evaluated and refined.

2. Materials

The model alloys used in this study were a Fe–0.80at.% Cu (VH) and a Fe–0.78 at.% Cu–1.05at.% Mn (VD). All compositions quoted in this paper are given in atomic percent. The alloys were solution treated for 17 h at 775 °C and then quenched in a salt bath at

* Corresponding author. Tel.: +1-865-574-4719; fax: +1-865-241-3650

E-mail address: millermk@ornl.gov (M.K. Miller).

0921-5093/02/$ - see front matter
PII: S0921-5093(02)00679-2

Table 1
Number of clusters found in simulations (60% detection efficiency) and atom probe analysis of unirradiated control materials for a maximum atom separation of 0.5 nm

Cluster size (atoms)	Number observed in AP	Frequency (%)		Solute in clusters (%)	
		APT VH	Simulation 0.80% solute	APT VH	Simulation 0.80% solute
1	8178	87.79	87.45	75.78	76.24
2	897	9.63	10.71	16.62	18.67
3	172	1.85	1.59	4.78	4.17
4	50	0.54	0.22	1.85	0.78
5	9	0.10		0.42	
6	6	0.06	0.03	0.33	0.15
7	2	0.02		0.13	
8	0				
9	1	0.01		0.08	
		APT VD	Simulation 1.83% solute	APT VD	Simulation 1.83% solute
1	10257	81.59	74.83	64.57	53.87
2	1675	13.32	17.06	21.09	24.56
3	439	3.49	4.80	8.29	10.37
4	117	0.93	1.94	2.95	5.60
5	44	0.35	0.77	1.38	2.77
6	23	0.18	0.41	0.87	1.78
7	6	0.05	0.11	0.26	0.57
8	4	0.03	0.04	0.20	0.26
9	3	0.02	0.02	0.17	0.15
10	1	0.01	0.01	0.06	0.08
11	1	0.01		0.07	
12	0				
13	1	0.01		0.08	

450 °C for 3 min and air-cooled to room temperature. Thermodynamic calculations predicted that no face-centered cubic ε-Cu precipitates formed at 775 °C [6]. These model alloys were neutron irradiated to a fluence of $\sim 1 \times 10^{23}$ nm^{-2} ($E > 1$ MeV) at a temperature of 288 °C.

3. Atom probe

The atom probe characterizations were performed in the Oak Ridge National Laboratory (ORNL) energy-compensated three-dimensional atom probe. Standard analysis conditions of a specimen temperature of 45 K, a pulse fraction of 20% of the standing voltage and a pulse repetition rate of 1.5 kHz were used [7]. The field factor k_F in the reconstruction procedure of the atom positions [1] was determined from transmission electron microscope measurements of the end radii of atom probe specimens with known best image/field evaporation voltages.

Atom probe analysis of the unirradiated materials yielded compositions of Fe–0.74±0.01% Cu for the VH alloy and Fe–0.65±0.02% Cu, 0.93±0.02% Mn for the VD alloy suggesting that some heterogeneous ε-Cu face-centered cubic precipitation occurred during the annealing treatment at 450 °C or that some preferential evaporation or pile-up of copper occurred during atom probe analysis [1]. Estimates of the copper compositions based on electrical resistivity and Seebeck coefficient measurements were somewhat higher at 0.77±0.05% Cu and 0.81±0.01% Cu for VD and VH, respectively [8]. No intergranular copper-enriched precipitates or clusters were observed in the atom probe or by transmission electron microscopy [9] in either unirradiated material. Atom probe analysis of the matrix of the neutron-irradiated materials yielded compositions of Fe–0.046±0.004% for the VH alloy and Fe–0.075±0.005% Cu, 0.96±0.02% Mn for the VD alloy. As expected, these results indicated that neutron irradiation substantially reduced the copper levels.

The distance between solute atoms in a solute-enriched cluster or precipitate is significantly smaller than that in the surrounding matrix. Therefore, the presence and extent of clusters were determined with the use of a method based on the maximum separation distance between Cu and Mn atoms [1,10]. Computer simulations of random solid solutions containing 0.80 and 1.83 at.% solute (i.e., the combined copper and manganese concentrations in the alloy) with a body-centered cubic crystal structure with the α-Fe lattice parameter ($a_0 = 0.288$ nm) and a detection efficiency of 60% were used to define the maximum separation distance between Cu and Mn atoms, d_{max}, and the

minimum number of solute atoms associated with clusters, n_{min}. These parameters were then validated with the use of APT analysis of unirradiated control specimens. The results for $d_{max} = 0.5$ nm are shown in Table 1 and indicate good agreement between the simulations and the atom probe data. These results indicate that no clusters containing more than 9 and 13 atoms were observed during atom probe analysis of the binary and ternary alloy, respectively, or more than 6 and 10 atoms in the simulations, respectively. Therefore, parameters of $d_{max} = 0.5$ nm and $n_{min} = 10$ atoms were used for the analysis of the 3DAP data from neutron-irradiated materials to exclude fluctuations consistent with the random solid solution. However, the atom probe data are able to characterize small clusters below these limits and they should be taken into account in a full description of the alloy and its mechanical properties.

Atom maps of the solute associated with the clusters in the neutron-irradiated binary and ternary alloys as defined by the maximum separation method are shown in Fig. 1. The number density of these clusters may be estimated from the number of clusters within the volume of analysis taking into account the partial sampling of clusters at the edge of the volume. The number densities of the clusters in the binary and ternary alloys were estimated to be $7 \pm 3 \times 10^{22}$ and $7 \pm 2 \times 10^{23}$ m^{-3}, respectively. It is evident that the number density of clusters is approximately an order of magnitude higher in the neutron-irradiated ternary alloy compared with the binary alloy indicating the large influence of manganese.

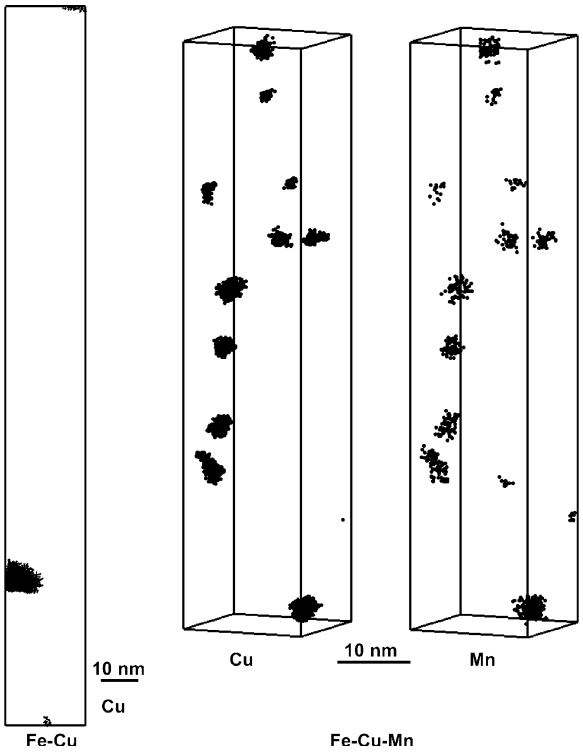

Fig. 1. Copper and manganese atom maps of the solute-enriched clusters in the neutron-irradiated Fe–Cu and Fe–Cu–Mn alloys. The matrix solute atoms have been eliminated based on the maximum separation method [1]. The number density of the clusters was an order of magnitude larger in the ternary alloy.

The center of mass and the radius of gyration, l_g, may be calculated from the spatial coordinates of each solute atom in the feature [1,4,5,10,11]. The average l_g for the binary and ternary alloys were estimated to be ~ 2.3 and 1.2 ± 0.4 nm, respectively. The precision of the estimates of the spatial positions of individual atoms is influenced by the reconstruction process and trajectory aberrations [1]. In addition, these raw estimates do not take into account differences in the local magnification between the clusters and the matrix (see below). For the Fe–Cu–Mn alloy, the radii of gyration based on the Cu and Mn atoms, $l_{g(Cu)}$ and $l_{g(Mn)}$, are compared with the l_g based on the Cu + Mn atoms in Fig. 2. The comparison indicates that $l_{g(Mn)}$ is larger than $l_{g(Cu)}$ and l_g. The extended Mn profile is also evident in radial composition profiles constructed with their origins positioned at the centers of mass, an example of which is shown in Fig. 3, and are in agreement with predictions of a Cu core surrounded by a Mn shell [12].

The compositions of these nanometer-scale clusters may be estimated by several methods. In the envelope method [1], a fine grid of volume elements around each feature is defined. The precise extents of the grid are based on the presence of a solute atom (Cu and Mn) within each volume element as defined by the maximum separation method. Due to the fine spacing of the grid (0.2 nm) which results in small numbers of atoms within each volume element, the volume elements in the interior of the feature that do not contain a solute atom are also included. The composition of the feature is then estimated from the total number of atoms of all

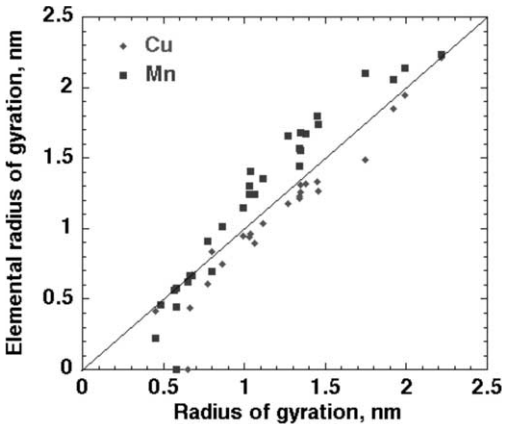

Fig. 2. A comparison of the copper and manganese radii of gyrations to the overall radii of gyration based on copper + manganese atoms. The manganese radii of gyration are generally slightly larger than the copper radii of gyration.

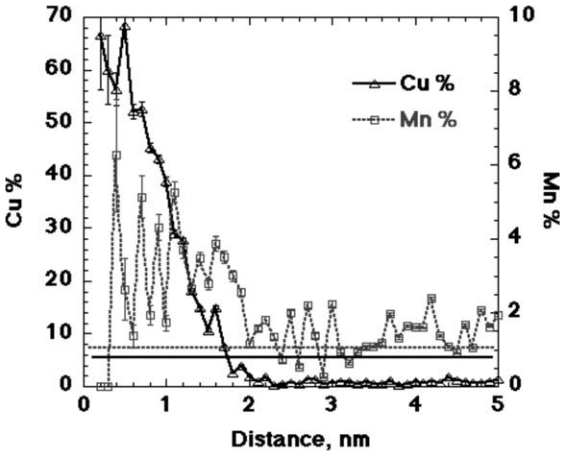

Fig. 3. Radial compositions from the center of mass of a solute-enriched feature revealing that the manganese distribution extends further from the center of the feature than the copper distribution.

the elements that are encompassed within the volume. The outer surface of the envelope may be eroded to minimize the contribution of the matrix solutes to the overall composition. One of the advantages of this envelope method is that it can be applied to irregularly shaped features. The composition of each feature may also be estimated from the number of atoms within a spherical shell positioned with its origin at the center of mass and its radius defined by either the l_g or the Guinier radius, r_G. The composition of the feature may also be estimated from the number of atoms in a small spherical or cuboidal volume element whose position is manually selected within the three-dimensional data. For the large precipitate in the Fe–Cu alloy data shown in Fig. 1, these methods yielded solute concentrations of $c_{env} = 49.9 \pm 0.7\%$ Cu, $c_{l_g} = 50.1 \pm 0.9\%$ Cu, $c_{r_G} = 39.2 \pm 0.6\%$ Cu and $c_{sel} = 73.0 \pm 0.7\%$ Cu, respectively. Due to the non-spherical nature of this precipitate, a significant contribution from matrix is included in the shell defined by the Guinier radius resulting in a lower average copper content. Composition profiles through this precipitate revealed significant local variations in the copper level. The selected volume was chosen to yield the highest local copper level, which originated in the central core of the precipitate. The compositions of individual precipitates in the neutron-irradiated Fe–Cu–Mn alloy are shown in Fig. 4. Some evidence of a size dependency is apparent in the measured compositions. The average compositions as determined by the different methods were $c_{env} = 35.5 \pm 12.6\%$ Cu, $10.3 \pm 6.6\%$ Mn, $c_{l_g} = 21.0 \pm 10.7\%$ Cu, $3.7 \pm 2.0\%$ Mn and $c_{sel} = 43.8\%$ Cu, 4.1% Mn for the copper-enriched clusters and $c_{env} = 7.2 \pm 5.6\%$ Cu, $49.1 \pm 4.5\%$ Mn, $c_{l_g} = 0.9 \pm 1.4\%$ Cu, $10.6 \pm 2.4\%$ Mn for the smaller ($l_g = 0.6 \pm 0.1$ nm) manganese-enriched clusters. The large standard deviations of these measurements are indicative of the wide variations in measured compositions and the non-equilibrium nature of the precipitates.

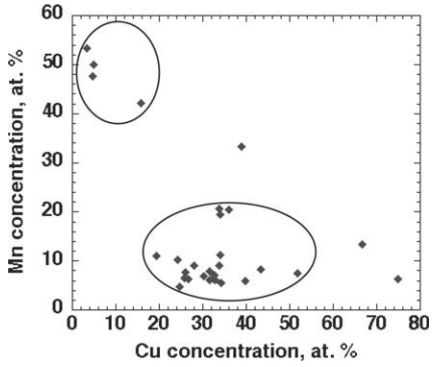

Fig. 4. The distribution in the compositions of the clusters in the neutron-irradiated Fe–Cu–Mn alloy. Two distinct composition fields are apparent in the data.

Differences in the local magnification between the precipitate and matrix regions are manifested in different apparent average local atomic densities measured by the envelope method. This additional information permits a correction to be made for the local magnification in the radius of gyration measurements [1]. The corrected average values of the radius of gyration are $l_g = 2.8$ and 1.8 nm for the neutron-irradiated Fe–Cu and Fe–Cu–Mn alloys, respectively.

4. Small-angle neutron scattering

The SANS experiments were performed at the National Institute of Standards and Technology (NIST) Center for Neutron Research (CNR) [13]. SANS arises from both nuclear (N) and magnetic (M) scattering length density differences between the ferrite matrix and the scattering feature [14]. Thus the specimens were measured in a strong (1.8 ± 0.1 T) magnetic field, which saturated the α-Fe matrix. The scattering at small angles ($\theta \leq 8^\circ$) from a well-collimated beam of ~ 0.5 nm wavelength neutrons was recorded on a position sensitive detector with a maximum q-range of ~ 3 nm^{-1}. Scattering data for the radiation-induced clusters were obtained by subtracting background counts, parasitic scattering and the normalized scattering of an unirradiated control specimen from the net scattering count recorded in each detector pixel. The corrected data were converted to absolute scattering cross-sections, $d\Sigma/d\Omega$, by normalizing to a water reference sample, including standard accounting for transmission and sample volumes. Finally, the cross-sections were averaged over small increments of q and the angle ϕ with respect to the magnetic field direction.

The scattering cross-sections were fitted to a log-normal size distribution of either one or two spherical feature(s) [2,15–17]. The mean size and width of the log-

normal size distributions are obtained from the shape (curvature) of the scattering cross-section data, whereas the number density (volume fraction) of clusters is obtained from the absolute magnitude of the scattering cross-sections and the known nuclear or magnetic scattering contrast. The main assumption in our SANS data analysis is that the Cu–Mn precipitates are spherical and non-magnetic features in a saturated ferromagnetic iron matrix, which fixes the magnetic scattering contrast to a precisely known value [18], and thereby allows absolute estimates of the number density and volume fraction of the non-magnetic scattering features. The measured ratio between the magnetic to nuclear (M/N) scattering then provides information about the composition of the scattering feature(s). The inverse square root of M/N, $\sqrt{\mathrm{N/M}}$, is a linear function of the precipitate composition as

$$\sqrt{\frac{\mathrm{N}}{\mathrm{M}}} = 1.58 - 1.58X_{\mathrm{Fe}} - 1.22X_{\mathrm{Cu}} + 0.59X_{\mathrm{Mn}} - 1.63X_{\mathrm{Ni}}, \quad (1)$$

where the X_i's are the composition fraction of the precipitates such that $X_{\mathrm{Fe}}+X_{\mathrm{Cu}}+X_{\mathrm{Mn}}+X_{\mathrm{Ni}}+X_{\mathrm{vac}}=1$. In the case of these binary and ternary Fe–Cu–Mn alloys, the M/N ratio provides a relatively clear indication of precipitate composition.

The precise numerical parameters of mean size and volume fraction derived from the fits with two features are not unique and are somewhat to strongly covariant, particularly when the sizes of the two features are similar. In addition to contributions from the covariance of two feature fits and the analysis assumptions noted above, a contribution to uncertainties of the SANS precipitate fit parameters may result from small differences between the sample and controls due to typical material inhomogeneities. However, these differences have little effect at large values of scattering cross-sections as were measured for the VH and VD alloys. Overall, the uncertainties, δ, are estimated to be: $\delta l_g = \pm 0.2$ nm; $\delta f = 0.02\%$; and $\delta N_v = 25\%$.

The results of the SANS analysis are summarized in Table 2 and the fits are shown in Fig. 5. A better least-squares fit to the data was obtained by the superposition of two log-normal size distributions, with different magnetic to nuclear scattering ratios and mean sizes. The number densities and the radii of gyration for the larger of the two features reveal that larger, less numerous precipitates are formed in the Fe–Cu than the Fe–Cu–Mn alloy. The SANS results are in generally good agreement with the APT estimates for both alloys, although the SANS sizes are slightly higher and the number densities slightly lower than determined from APT.

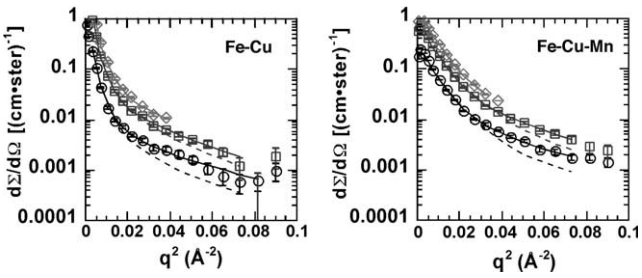

Fig. 5. Small-angle scattering $d\Sigma/d\Omega(q,\phi)$ defect cross-sections (symbols) and fit results (lines) at $0\pm30^\circ$ (circles), $45\pm15^\circ$ (squares) and $80\pm10^\circ$ (diamonds) with respect to the applied magnetic field, showing the one (dashed lines) and two (solid lines) feature fits.

The measured magnetic to nuclear scattering ratio of the precipitates is lower in the Fe–Cu–Mn (4.6) than the Fe–Cu (6.7) alloy. This reduction is consistent with the addition of manganese to the precipitates. The M/N ratio is not unique and indeed, as can be estimated from Eq. (1), a range of precipitate compositions are consistent with a given M/N scattering ratio. Magnetic measurements [19], along with analytical considerations [12], suggest that precipitates containing more than 30% Fe will have a non-zero magnetic moment, and thus, only the scattering ratios for $X_{\mathrm{Fe}} \leq 30\%$ were calculated. In the Fe–Cu alloy, the M/N ratio of 6.7 is consistent with a composition of 98% Cu, 2% vacancies and no Fe, as well as 72% Cu, 8% vacancies and 20% Fe. In the Fe–Cu–Mn alloy, the M/N ratio of 4.6 is consistent with a composition of 94% Cu, 6% Mn and no Fe or vacancies, as well as 70% Cu, 10% Mn and 20% Fe with no vacancies. Increasing the precipitate vacancy concentration results in slightly reduced Mn and Cu concentrations, e.g., 5% vacancies require compositions of 92% Cu, 3% Mn with 0% Fe or 69% Cu, 6% Mn with 20% Fe

Table 2
SANS radius of gyration and number density results for a one and two feature fit

		l_g (nm)	N_v (m^{-3})	F (%)	M/N
Fe–0.80% Cu	One feature fit	3.5	5×10^{22}	0.88	6.7
	Two feature fit	3.4	4.6×10^{22}	0.75	6.7
		0.9	1.2×10^{23}	0.04	1.5
Fe–0.78% Cu–1.05% Mn	One feature fit	1.8	3.5×10^{23}	0.89	4.6
	Two feature fit	2.0	2.3×10^{23}	0.78	4.6
		0.95	3.0×10^{23}	0.11	2.0

for an M/N of 4.6. However, it is important to note that Eq. (1) will overestimate the Fe content of precipitates containing vacancies, since the vacancies will most certainly relax the lattice strains and reduce the precipitate atomic volume (~ 12.5 Å^3 per atom) used in the derivation.

Although precipitate compositions with relatively large ($\sim 20\%$) Fe concentrations can yield M/N ratios consistent with the SANS measurements, such Fe concentrations are at odds with Fe–Cu alloy thermodynamics [12] and other measurement techniques, including combined electrical resistivity and Seebeck coefficients [8] and positron annihilation spectroscopy [17]. A better comparison between the APFIM and SANS compositions results from using the compositions obtained from the atom probe data to directly calculate the SANS M/N ratio, where $X_{Fe} \lesssim 33\%$, as well as to calculate the precipitate number densities (volume fractions) using the nuclear scattering contrast calculated for a given composition. For example, in the Fe–Cu alloy, a precipitate composition of 73% Cu and 27% Fe results in a magnetic to nuclear scattering ratio of about 14.5, considerably higher than the measured value of 6.7. In this case, calculation of the nuclear scattering contrast (thereby neglecting any assumptions of precipitate magnetization) requires a precipitate volume fraction of 1.5% to fit the nuclear scattering cross-sections, which involves more precipitated Cu ($1.5\% \times 0.73 \sim 1.1\%$) than is available in the Fe–Cu alloy. For the Fe–Cu–Mn alloy, the estimated precipitate composition of 44% Cu, 4% Mn and 52% Fe would likely result in a partially magnetic precipitate, making calculation of the M/N difficult. However, matching the measured nuclear scattering cross-sections to the calculated nuclear scattering contrast results in a precipitate volume fraction of $\sim 1.8\%$, again requiring more Cu than available in the alloy.

Thus, whereas the SANS results cannot discount some ($\sim 10\%$) Fe within the precipitates, they are not consistent with much higher levels of Fe (27–52%) and therefore, the SANS results indicate the precipitates are significantly more enriched in Cu than the APT results.

5. Conclusions

High number densities of ultrafine copper-enriched precipitates were observed in all materials after neutron irradiation. In the neutron-irradiated Fe–Cu–Mn alloy, manganese was also found in the copper-enriched precipitates, in agreement with theoretical predictions of a copper core surrounded by a manganese shell, and the number density of precipitates was approximately an order of magnitude higher and their size was smaller than in the similar Fe–Cu alloy. A direct comparison of the microstructural parameters estimated by APT and SANS revealed generally good agreement for the mean precipitate size and number density, but the precipitate compositions from the SANS analysis were significantly more enriched in Cu than from APT analysis.

Acknowledgements

The authors would like to acknowledge the contributions of Drs. S.S. Babu, E.A. Kenik and K.F. Russell (ORNL), D. Klingensmith (UCSB), Dr. J.M. Hyde (AEA Technologies) and Drs. J. Barker and C. Glinka (NIST) as well as the support of the National Institute of Standards and Technology, US Department of Commerce, in providing the neutron research facilities. Research at the Oak Ridge National Laboratory SHaRE Collaborative Research Center was sponsored by the Division of Materials Sciences and Engineering, US Department of Energy, under contract DE-AC05-00OR22725 with UT-Battelle, LLC, and by the Office of Nuclear Regulatory Research, US Nuclear Regulatory Commission under inter-agency agreement DOE 1886-N695-3W with the US Department of Energy. This research was also performed under the auspices of the US Department of Energy and Lawrence Livermore National Laboratory under contract No. W-7405-Eng-48 and at UCSB supported by the US Nuclear Regulatory Commission under contract number NRC-04-94-049.

References

[1] M.K. Miller, Atom Probe Tomography, Kluwer Academic Publishers/Plenum Press, New York, 2000.
[2] G.R. Odette, G.E. Lucas, Radiat. Eff. Defects Solids 144 (1998) 189.
[3] M.K. Miller, P. Pareige, M.G. Burke, Mater. Characterization 44 (2000) 235.
[4] M.K. Miller, P. Pareige, in: G.E. Lucas, L.L. Snead, M.A. Kirk, R.G. Elliman (Eds.), Microstructural Processing Irradiated Materials—2000, vol. 650, Materials Research Society, Pittsburgh, PA, 2001, p. R6.1.1.
[5] J.M. Hyde, C.A. English, in: G.E. Lucas, L.L. Snead, M.A. Kirk, R.G. Elliman (Eds.), Microstructural Processing Irradiated Materials—2000, vol. 650, Materials Research Society, Pittsburgh, PA, 2001, p. R6.6.1.
[6] The thermodynamic predictions were computed with the use Thermocalc™, N. Saunders, ThermoTech Ltd., Surrey Technology Centre, 40 Occam Road, The Surrey Research Park, Guildford, GU2 5YH, UK.
[7] M.K. Miller, K.F. Russell, P. Pareige, M.J. Starink, R.C. Thomson, Mater. Sci. Eng. A 250 (1998) 49.
[8] G.R. Odette, C. Cowan, D. Gragg, in: G.S. Was (Ed.), Proceedings of the 10th International Conference on the Environmental Degradation of Materials in Nuclear Power Systems–Water Reactors, Lake Tahoe, NV, August 5–9 2001, National Association of Corrosion Engineers (NACE) International, Houston, TX, 2002.
[9] H. Ruoff, personal communication.

[10] J.M. Hyde, Doctoral Thesis, University of Oxford, Oxford, 1993.
[11] M.K. Miller, K.F. Russell, P. Pareige, in: G.E. Lucas, L.L. Snead, M.A. Kirk, R.G. Elliman (Eds.), Microstructural Processing Irradiated Materials—2000, vol. 650, Materials Research Society, Pittsburgh, PA, 2001, p. R3.15.1.
[12] G.R. Odette, C.L. Liu, B.D. Wirth, MRS Symp. Proc. 439 (1997) 457.
[13] C.J. Glinka, J.M. Rowe, J.G. laRock, J. Appl. Crystallogr. 19 (1986) 427.
[14] G. Kostorz (Ed.), Newton Scattering, Treatise on Materials Science and Technology, Vol. 15, Academic Press, New York, 1979.
[15] J.A. Fint, Masters Thesis, University of California, Santa Barbara, CA, 1990.
[16] B.D. Wirth, W.A. Pavinich, G.R. Odette, G.E. Lucas, S. Spooner, in: R.K. Nanstad, M.L. Hamilton, F.A. Garner, A.S. Kumar (Eds.), Effects of Radiation on Materials: 18th Symposium, ASTM STP 1325, American Society for Testing and Materials, p. 102.
[17] B.D. Wirth, P. Asoka-Kumar, R.H. Howell, G.R. Odette, P.A. Sterne, in: G.E. Lucas, L.L. Snead, M.A. Kirk, R.G. Elliman (Eds.), Microstructural Processing Irradiated Materials—2000, Materials Research Society, Pittsburgh, PA, 2000, p. R.6.5.1.
[18] M.H. Mathon, Doctoral Dissertation, University of Paris-Sud, Paris, France, 1995.
[19] K. Sumiyana, T. Yoshitake, Y. Nakamura, J. Phys. Soc. Jpn. 53 (1984) 3160.